Climate Dynamics
https://doi.org/10.1007/s00382-019-05075-7

# Seasonal forecasting of tropical cyclones in the North Indian Ocean region: the role of El Niño-Southern Oscillation

**Md Wahiduzzaman[1,2] · Eric C. J. Oliver[3,4] · Simon J. Wotherspoon[2,5] · Jing-Jia Luo[1]**

Received: 26 June 2019 / Accepted: 2 December 2019


**Abstract**
In this study, we have investigated the contribution of El Niño-Southern Oscillation (ENSO) to the North Indian Ocean (NIO) tropical cyclone (TC) activity and seasonal predictability. A statistical seasonal prediction model was developed for the NIO region tropical cyclone genesis, trajectories and landfalls using the Southern Oscillation index (SOI: as a metric of ENSO) as a predictor. The forecast model utilised kernel density estimation (KDE), a generalised additive model (GAM), Euler integration, and a country mask. TCs from the Joint Typhoon Warning Centre were analysed over the 35-year period from 1979 to 2013. KDE was used to model the distribution of cyclone genesis points and the cyclone tracks were estimated using the GAM, with velocities fit as smooth functions of location according to ENSO phase and TC season. The best predictor lead time scales for TC forecast potential were assessed from 1 to 6 months. We found that the SOI (as a proxy for ENSO) is a good predictor of TC behaviour 2-months in advance (70% skill). Two hindcast validation methods were applied to assess the reliability of the model. The model was found to be skillful in hindcasting NIO region TC activity for the pre and post monsoon season. The distribution of TC genesis, movement and landfall probabilities over the study period, as well as the hindcast probabilities of TC landfall during ENSO events, matched well against observations over most of the study domain. Overall, we found that the phase of ENSO has the potential to improve NIO region TC seasonal forecast skill by about 15% over climatological persistence.

**Keywords** Tropical cyclones · El Niño-Southern Oscillation · Seasonal forecasting · Statistical modelling · North Indian Ocean

## 1 Introduction

Landfalling tropical cyclones (TCs) can be potentially catastrophic to human society, particularly along densely populated coastlines, such as along the rim of the North Indian Ocean (NIO). TCs can cause a substantial loss of life and very often cause significant damage to properties (Vissa et al. 2013; Balaguru et al. 2014; Wahiduzzaman and Yeasmin 2019a, b). In the NIO region, there have been devastating losses due to TCs that make landfall, including in recent years (Pattanaik and Mohapatra 2016). In 2008, 138,000 people lost their lives and US$10 billion damages were caused by Cyclone *Nargis* (Webster 2008; Alam et al. 2003). Aside from the clear costs to human life, TCs also pose a substantial monetary risk to reinsurance enterprises (Rumpf et al. 2007).

Skillful seasonal forecasting of tropical cyclone activity has the potential to aid decision-makers, planners and coastal inhabitants to take potential action months

✉ Jing-Jia Luo
jjluo@nuist.edu.cn

1 Key Laboratory of Meteorological Disaster of Ministry of Education/Collaborative Innovation Center on Forecast and Evaluation of Meteorological Disasters/Institute for Climate and Application Research (ICAR), Nanjing University of Information Science and Technology, Nanjing, China

2 Institute for Marine and Antarctic Studies (IMAS), University of Tasmania, Hobart, TAS, Australia

3 Department of Oceanography, Dalhousie University, Halifax, NS, Canada

4 Australian Research Council Centre of Excellence for Climate Extremes, Hobart, TAS, Australia

5 Australian Antarctic Division, Kingston, TAS, Australia

Published online: 31 December 2019

in advance. For governments, skillful seasonal forecasting is likely to aid both planning and decision-making. To develop skillful TC seasonal forecasts, it is essential to know the significant factors that affect TC formation, tracks, and landfall. Because of a deficiency of observations and resources, seasonal forecast skill of TCs in the NIO region remains relatively poor. A few studies have examined the effect of the atmospheric and oceanic states on the variation of TC activity in the Bay of Bengal (Sengupta et al. 2007; Girishkumar and Ravichandran 2012; Felton et al. 2013; Wahiduzzaman et al. 2017). These studies have not, however, considered El Niño-Southern Oscillation (ENSO) as a key predictor in statistical seasonal forecasts of tropical cyclones. Even dynamical models, such as the UKMO Glosea5, have been unable to forecast the phase relationship between ENSO and TCs in the Bay of Bengal (e.g. Camp et al. 2015) and more generally in the NIO region.

ENSO is the dominant ocean–atmosphere phenomenon in the Tropical Indo-Pacific and affects the large-scale climate globally (An et al. 2007; Ashok and Saji 2007; Chand and Walsh 2011; Werner et al. 2012; Hsu et al. 2013; Camp et al. 2015; Wang et al. 2018; Zhao et al. 2019). Generally, the duration of a single ENSO event (either El Niño or La Niña) is 1.5–2 years phase-locked to the seasonal cycle with a quasi-periodic frequency of occurrence on average every 2–8 years. It is the coupling between sea level pressure, expressed as the winds and wind stress, and eastern equatorial Pacific sea surface temperature anomalies associated with ENSO, as well as its timing and spatial teleconnections, that are responsible for how ENSO drives large-scale changes in climate variations and extremes across the globe. The effect on tropical cyclones are felt in various ocean basins including the Pacific, Atlantic and Indian Oceans (Chu 2004; Zhang et al. 2012; Du et al. 2013; Camp et al. 2015). The relationship between tropical cyclones and ENSO has been examined by Ho et al. (2006), Kuleshov et al. (2008), Girishkumar et al. (2012, 2014), Srikanth et al. (2012), Felton et al. (2013), Camp et al. (2015), Girishkumar et al. (2015) and Mahala et al. (2015) in the NIO basin.

Related studies on TCs and ENSO over the Bay of Bengal (BoB) have also been undertaken. Singh et al. (2001) examined the relationship between ENSO and the activity of tropical depressions in the BoB during the summer monsoon season (July–August), and found there were more tropical depressions during El Niño years. In another study, Singh et al. (2000) showed that there was a reduction in cyclonic storms in the two peak seasons (pre- and post-monsoon) over the BoB during El Niño years. Camargo et al. (2007) demonstrated the influence of ENSO on the genesis potential index (useful metric for gauging the performance of global climate models to simulate TC genesis) in all ocean basins and found a shift of genesis from the northern to the southern part of the BoB due to wind shear difference between La Niña and El Niño years.

Seasonal forecasting of tropical cyclone landfall by dynamical models is challenging (Camargo 2013; Camp et al. 2015) and its skill varies with model (Camargo et al. 2005; Bengtsson et al. 2007; Camargo and Barnston 2009). For example, the GLOSEAS model has previously shown little accuracy in the simulation of the seasonal cycle of TCs over the NIO region (Camp et al. 2015). Other dynamical models, including the Dynamical High Resolution Model, Consortium for small Scale Modelling and Artificial Neural Network System models, have also been shown not to forecast tropical cyclone landfall well because of limited spatial resolution and number of simulations.

Several previous studies (Klotzbach 2011; Girishkumar and Ravichandran 2012; Felton et al. 2013; Li and Zhou 2013) have shown that climate parameters relevant to TCs vary substantially with ENSO. However, a few studies have investigated TC frequencies and trajectories in the BoB and their relationship with ENSO (Girishkumar and Ravichandran 2012; Ng and Chan 2012; Felton et al. 2013; Mahala et al. 2015), but no study was found about the development of a statistical prediction model, using ENSO as the predictor variable, to simulate TCs tracks and forecast landfall in advance. We develop such a model, following a similar approach to that which was undertaken to model TC activities using the quasi-biennial oscillation as predictor, and explained by Wahiduzzaman et al. (2019).

Our paper is outlined as follows. The model description and data are provided in Sect. 2. A lead–lag analysis is also presented in this section. The results are discussed in Sect. 3, and a summary and discussion are delivered in Sect. 4.

## 2 Methodology

Previous statistical models of TC tracks and TC genesis (James and Mason 2005; Emanuel et al. 2006; Rumpf et al. 2007; Hall and Jewson 2007; Yonekura and Hall 2011) have been beneficial in generating sets of synthetic TCs that are much larger than the limited numbers in historical observations. These models compute the direction of tracks from the synthetic sets by using kernel density estimation and autoregressive modelling. Wahiduzzaman et al. (2017, 2019) developed a climatological and forecast model for the NIO (Fig. 1) TC activities closely following the approaches of Hall and Jewson (2007) and Yonekura and Hall (2011).

Here, we again apply similar approaches but using the Southern Oscillation index (as a metric for ENSO) as a predictor. The procedure for the simulation of TC trajectories is two-fold. First, TC genesis points are sampled from a spatial probability density function that has been calculated by kernel density estimation. Second, the TC track "velocity

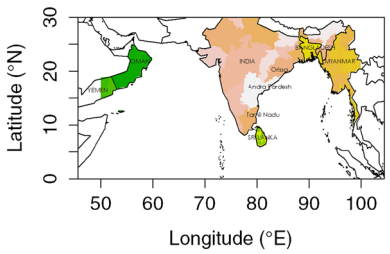


**Fig. 1** North Indian Ocean (0°–30° N and 50° E–100° E) rim countries (figure reproduced from Wahiduzzaman et al. 2017)

field" was generated by calculating latitudinal and longitudinal differences between observed TC positions in time along the observed cyclone tracks, and a Generalised Additive Model model was fitted to model the observed "velocity field" within a season and ENSO phase. The predicted velocity was then used to model TC trajectories from the genesis point and generate the modelled TC tracks. This was performed jointly for each ENSO phase (El Niño, La Niña) and season-Winter (Dec–Feb); Pre-monsoon (March–May); Monsoon (Jun–Sep) and Post-monsoon (Oct–Nov). The trajectories are based on a maximum lifespan of 7 days and a 6-h step interval. From this model, a number of synthetic but realistic storm tracks were simulated and these synthetic track statistics are used to generate probabilistic landfall hazard zone maps.

## 2.1 Tropical cyclone data

The International Best Track Archive for Climate Stewardship (IBTrACS) dataset was established by the NOAA National Climatic Data Center to integrate the best TC track data from all official Tropical Cyclone Warning Centres (TCWCs) and the WMO Regional Specialized Meteorological Centres (RSMCs). These data were obtained from http://www.ncdc.noaa.gov/oa/ibtracs/. The data have been used from the Joint Typhoon Warning Centre (JTWC), a subset of IBTrACS from 1979 to 2013 (35-year)—with the data since 1979 being more reliable (e.g. Wahiduzzaman et al. 2017). The JTWC data have been used by most researchers studying TCs in the NIO (Knapp et al. 2010).

## 2.2 Southern Oscillation Index

The Southern Oscillation Index (SOI) is defined as the sea level pressure difference between Tahiti and Darwin (Ropelewski and Jones 1987) and is a useful metric often used to describe ENSO variations. The SOI has been used in numerous previous studies to examine and model the role of ENSO on TC activity in the tropical southwest Pacific and eastern Indian Ocean as well as the northwest Pacific. The SOI varies on subannual, and interannual to multidecadal timescales. The data in this study were smoothed by averaging a 3-month period.

The form of the SOI used here follows the Australian Bureau of Meteorology (Troup 1965), that is the SOI used is the standardised anomaly of the mean sea level pressure (MSLP) difference between Tahiti and Darwin:

$$SOI = 10\frac{P_{diff} - P_{avgdiff}}{SD(P_{diff})},$$

where $P_{diff}$ = (average Tahiti MSLP for the month) − (average Darwin MSLP for the month), $P_{avgdiff}$ = long term (60 years climatology period) average of $P_{diff}$ for the month in question, and $SD(P_{diff})$ = long term standard deviation of $P_{diff}$ for the month in question. A sustained value of the SOI below −7 indicates El Niño while sustained values above +7 indicate La Niña conditions. The SOI was obtained from http://www.bom.gov.au/climate/current/soihtm1.shtml.

## 2.3 TC genesis, track and landfall model

Using a 30-year record of TC observations (1980–2009) and SOI data (1979–2009), the genesis points have been modelled by kernel density fitting. The cyclone paths were simulated using a Generalised Additive Model. Trajectories are then simulated by drawing new random genesis points from the fitted kernel density estimates and tracing the cyclonic paths from the fitted velocity fields and then determined the point of landfall. The model was validated and assessed to measure the forecast skill.

### 2.3.1 Kernel density estimation for genesis

The spatial allocation of tropical cyclone genesis points was modelled using kernel density estimation (KDE). The KDE used here is outlined by Wahiduzzaman et al. (2017) and Wahiduzzaman and Yeasmin (2019a, b). The estimator convolves the data with the Gaussian kernel function to make a smooth approximation of the data density—here, specifically representing the spatial distribution of tropical cyclone genesis occurrences. The degree of smoothing is controlled by the plug-in "bandwidth" of the kernel.

To define the genesis locations, we identify those tropical storms in the data when wind speeds first exceed 34 knots. The spatial distribution of genesis points was then estimated for each season and ENSO phase with a kernel density estimator using a two-dimensional Gaussian kernel and a simple plug-in estimator for the optimal bandwidth (Rigollet and Vert 2009). To generate simulated samples of TC genesis locations we draw randomly from the estimated Probability Density Function.

#### 2.3.2 Trajectories model

Cyclone tracks were modelled by fitting a Generalised Additive Model (GAM) to the observed trajectory velocities. The GAM is a generalisation of linear regression in which the linear relationships are changed by smooth changes of the predictors.

Linear regression acts to model $\mu$ (the expected value) or $Y$ (dependent variable)

$$\mu = E(Y|X_1, X_2, \ldots, X_p) = \beta_0 + \beta_1 X_1 + \beta_2 X_2 + \ldots \beta_p X_p,$$

where $\beta_0, \beta_1, \ldots, \beta_p$ are the regression coefficients and $X_1$, $X_2$, …, $X_p$ are the variables. These variables are substituted by smooth transformations of the predictors in the GAM as

$$\mu = E(Y|X_1, X_2, \ldots, X_p) = \beta_0 + f_1(X_1) + f_2(X_2) + \ldots f_p(X_p).$$

the GAM estimates the smooth transformations $f_1, f_2, \ldots, f_p$. Typically, these functions do not have an easily represented parametric form.

Details of the GAM implemented here is also outlined by Wahiduzzaman et al. (2017). For the present application, the GAM was fitted to the observed tropical storm track velocities, for each combination of season and ENSO phase. Storm track velocities were calculated by differencing the latitudinal and longitudinal positions of the storms to generate velocities along the track increments. Since close to 80% of the TC lifespans in the NIO area are seen within 7 days from TC formation, capping at 7-day TC lifetimes (4-time/day) was seen to be a realistic selection for the model (Wahiduzzaman et al. 2017).

#### 2.3.3 Landfall model

For each simulated track, a landfall determination was made by analysing the track against the country mask ($1/12^0$) outline. To determine the place and time of landfall, each trajectory was also interpolated to a finer time scale and successive points along this fine-scale trajectory were compared to the raster land mask, with the first point to fall on land considered to be the point of landfall. We have not considered multiple landfalls as these are hardly seen in the NIO region (Wahiduzzaman et al. 2017).

### 2.4 Model validation

Two validation methods were applied in this study. Firstly, leave-one-out cross-validation was implemented by eliminating each trajectory one by one and then predicting this trajectory from the model fit to the remaining data set. Secondly, the distance between the observed and predicted landfalls have been calculated from the TC trajectories. For every observed landfall, a number of tracks originating from the same genesis point as the observed track were simulated, and then histograms of the distance were constructed and evaluated.

### 2.5 Lead–lag analysis

Lead–lag analysis has been presented by following two approaches to evaluate the best predictor timescale for the ENSO. The first was based on the distance calculation, and the second based on the comparison of landfall between observed and the simulated country (determined by majority vote). Table 1 shows the percentage of simulated landfall within 500 km of the observed landfall by lead month, and this percentage was converted to a skill score by decile. The highest percentage (i.e. 66.5%, representing a skill score in decile 7) was found for the 2-month lead SOI as predictor of landfall. However, the model has utility also with 5- and 6-month SOI leads (skill score in decile 6), but performs worst for 3- and 4-month leads.

Table 2 compares the observed number of TC landfalls with the model predicted landfalls from the simulated tracks for each lead month and informed by ENSO phase. In general, the model under-predicts landfall percentage totals in Bangladesh and consistently over-predicts landfall percentage totals in India and Sri Lanka. As the NIO rim countries have very different sizes and geometries, we chose to focus on point of landfall rather than country of landfall and chose the 2-month lead SOI as predictor variable.

## 3 Results

### 3.1 Modelling of TC genesis and track

The highest average frequency of genesis (Fig. 2) is observed in La Niña years (3.67/year), whereas El Niño and the Neutral years correspond to the 2.9 and 2.76 respectively over the NIO. These results are consistent with those of

**Table 1** For each lead month, the difference between observed and simulated tropical cyclones landfall is shown

| Lead month | TC landfall (in percentage) | Skill |
|---|---|---|
| 1 | 47.9 | 5 |
| 2 | **66.5** | 7 |
| 3 | 22 | 3 |
| 4 | 24.1 | 3 |
| 5 | 53.5 | 6 |
| 6 | 53.5 | 6 |

The highest skill is denoted by the bold percentage. A skill score of 1 corresponds to 1–10% predicted (decile 1) so that a skill score of 10 corresponds to 91–100% (decile 10)

**Table 2** For each lead month, the observed and simulated tropical cyclones landfall frequency as ENSO predictor is shown. For each country, the bold number highlights the best lag and the failure simulation in that lead month is denoted by bold with underlined percentages

| Country | Observed landfall (in number) | Month-1 (simulated number) | Month-2 (simulated number) | Month-3 (simulated number) | Month-4 (simulated number) | Month-5 (simulated number) | Month-6 (simulated number) |
|---|---|---|---|---|---|---|---|
| India | 34 | 52 | 53 | 20 | **37** | 45 | 59 |
| Myanmar | 7 | 1 | 5 | **8** | 12 | 11 | 3 |
| Bangladesh | 14 | **0** | **2** | **0** | 1 | **0** | **0** |
| Sri Lanka | 3 | 7 | **2** | 17 | 7 | 9 | 5 |
| Yemen | 0 | 7 | 4 | **0** | 2 | 4 | 3 |
| Oman | 5 | 8 | 11 | 1 | **6** | 4 | 16 |
| NON | 25 | 13 | 11 | 41 | **23** | 15 | 2 |

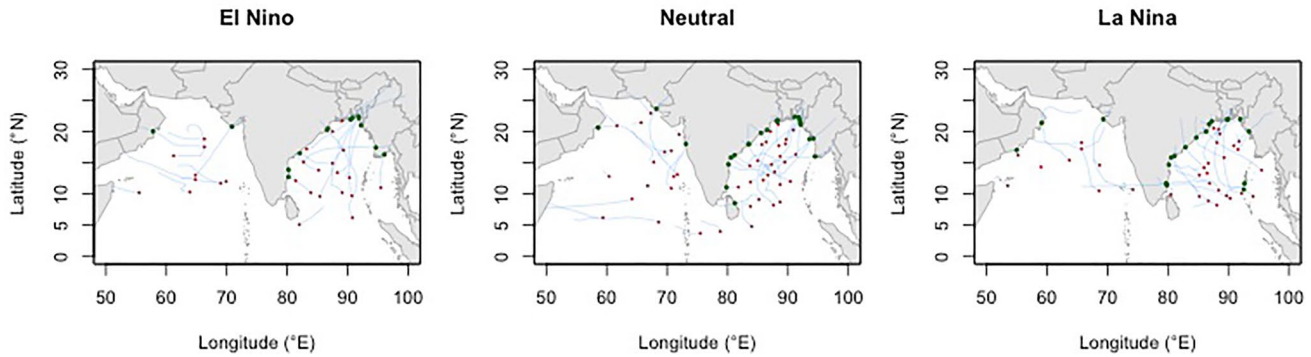


**Fig. 2** Observed TC genesis, trajectories and landfall for El Niño (left), Neutral (middle) and La Niña (right) phases of the ENSO in the 30-year period from 1980 to 2009 (El Niño, Neutral and La Niña phases consist 24%, 58% and 18% seasons respectively). Red (green) dots show the genesis (landfall) point in the NIO region (0°–30° N and 50°–100° E) and the blue lines specify the trajectories

Girishkumar and Ravichandran (2012), Felton et al. (2013) and Mahala et al. (2015) over the BoB. During El Niño, TCs are moving towards westward and northward over the BoB and make landfall in Tamil Nadu (India), Chittagong (Bangladesh), and Irrawaddy (Myanmar). During the Neutral phase of ENSO, most BoB TCs track towards the west (and make landfall into the Andhra Pradesh and Orissa states of India) and the north (and make landfall along the eastern part of Bangladesh) and few of them along the Irrawaddy coast of Myanmar. During La Niña, the TCs are moving towards the northwest in the BoB and make landfall along the northeast coast of India and Bangladesh. Over the Arabia Sea, TCs are moving towards Oman during El Niño and the ENSO Neutral phase. In short, during the El Niño phase, a large number of cyclones make landfall south of 17° N. Conversely, during La Niña and the Neutral phase, TCs make landfall in the north of 15° N. The tracks shown in Fig. 2 are consistent with previous TC observation reports by Girishkumar and Ravichandran (2012), Felton et al. (2013) and Mahala et al. (2015) over the BoB. Interestingly, we note a much greater number of TCs have been observed to form in the Arabian Sea during El Niño than in La Niña over the 35-year record (see Fig. 2).

The modelled distribution of TC genesis points, assessed by KDE, is shown in Fig. 3. For each phase of ENSO, the highest densities are observed in the Bay of Bengal. In the Neutral phase, the highest density is seen between 7 and 21° N in the Bay of Bengal and 10–15° N in the Arabian Sea. In the El Niño phase, the highest densities are between 10–17° N in the Bay of Bengal and 10–13° N in the Arabian Sea. Finally, in the La Niña phase, it is in 10°–20° for the Bay of Bengal and 15°–18° in the Arabian Sea.

Figure 4 shows the frequency distribution of 7 days from TC genesis to landfall, according to ENSO phase. Highest landfall rates are observed from 0 to 2 days after genesis in the La Niña phase (86% of the time). During the Neutral phase TC landfall tends to occur 1–2 days after genesis (75.6%). During El Niño, close to 50% (51.1%) of TCs made landfall within 0–1 day after genesis.

The GAM fits to the observed TC tracks for each ENSO phase are shown in Fig. 5. In the Arabian Sea, during either the El Niño or ENSO Neutral phase, the gridded Eulerian (vector) field is predominantly westward in the south and more northwestward in the north. During La Niña, there is a more apparent eastward component of the motion. In the BoB during the La Niña and Neutral

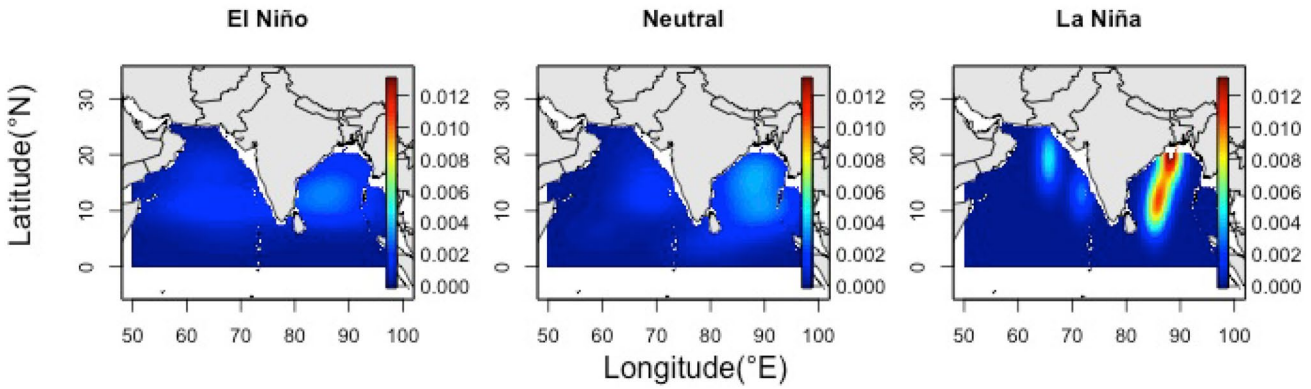


**Fig. 3** TC genesis modelling from 1980 to 2009 based on KDE for the El Niño (left), Neutral (middle) and La Niña (right) phases of the ENSO. The highest density (concentration of TC numbers/km$^2$) area of genesis is marked by red color

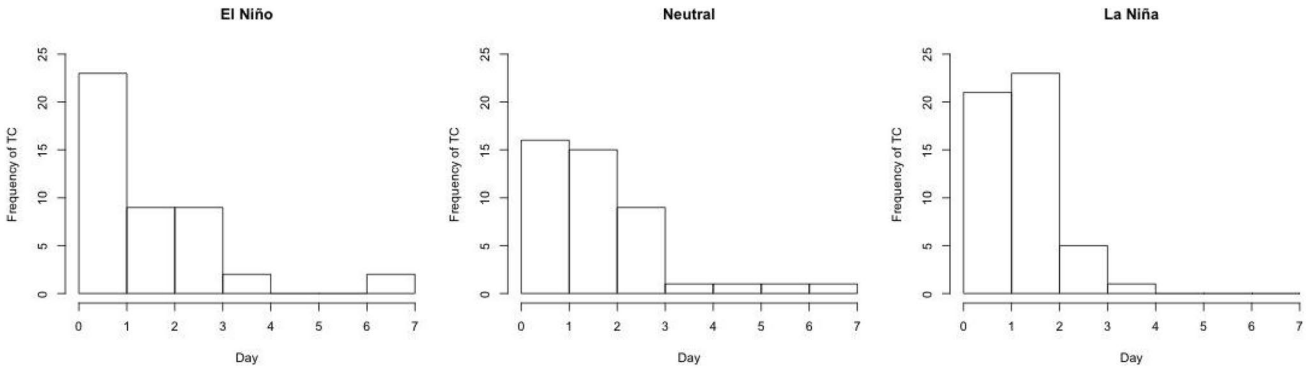


**Fig. 4** Observed TC landfall frequency distribution from TC genesis to landfall within 7 days

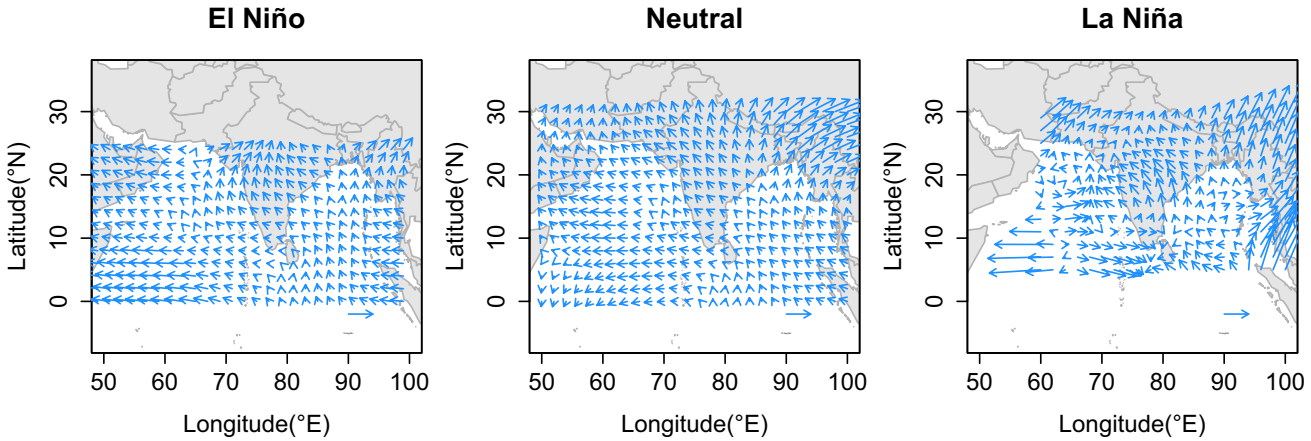


**Fig. 5** Velocities of TC track during El Niño, Neutral and La Niña phase. Reference arrow denotes 10m/s

phases, the vector field is predominantly northeastward in the south, with cyclones more strongly directed to Sri Lanka and the tip of India in La Niña. In the North of the BoB, the motion is predominantly northwest in the west and northeast in the east, becoming increasingly so in the Neutral and La Niña phases.

## 3.2 Model simulations

Model simulations (Fig. 6) show the movement of TCs and their point of landfall. In El Niño phase, tropical cyclones move towards west and northwest direction over the BoB with few exceptions and majority make landfall in the state

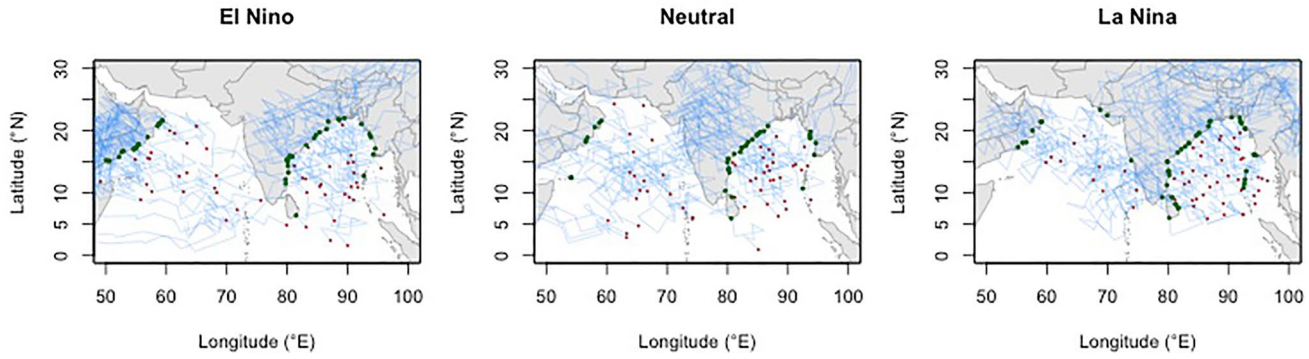


**Fig. 6** Simulated TC formation, movement and landfall during the El Niño (left), Neutral (middle) and La Niña (right) phases of the ENSO. Red (green) dots show the TC genesis (landfall) point in the NIO region (0°–30° N and 50°–100° E) for a 30-year period from 1980 to 2009. The blue lines direct the TC trajectories

of Tamil Nadu and Orissa of India; the southwestern zone of Bangladesh; and the state of Arakan and Irrawaddy of Myanmar. This is generally consistent with observations. Over the Arabia Sea, storms move towards the northwest and they make landfall in the state of Salalah and Sor of Oman and Yemen. During the neutral phase, many TCs move towards the northwest over the BoB and make landfall along the Andhra Pradesh of India and Irrawaddy of Myanmar. Over the Arabia Sea, storms move towards the northwest and make landfall in Oman (consistent with observations except the south-eastern part of Bangladesh). During the La Niña phase, storms move towards the northwest in the BoB and make landfall along the east coast of India, south-eastern part of Bangladesh and eastern part of Sri Lanka. Over the Arabia Sea, cyclones move towards the north and east direction (consistent with observations).

In Fig. 7, the frequency of simulated landfall is discussed according to time after genesis for all ENSO phase. The maximum frequency is seen around 1 day after genesis in La Niña phase (61.2% of the time), El Niño phase (51.1% of the time) and the Neutral phase (44.7% of the time). The simulated landfall exhausted earlier compare to observations.

### 3.3 Seasonwise tropical cyclone activities

Tropical cyclones develop frequently during the post-monsoon (Oct–Nov) season (Fig. 8) and the pre-monsoon (Mar–May) has approximately half of post-monsoon. Winter (Dec–Feb) and the monsoon season (Jun–Sep) are the quietest seasons. During post-monsoon season, most of TCs move westward and northwestward, and landfall is seen in the north-western and western portion of the BoB. However, in pre-monsoon season they move northeastward and landfall is seen in the north-eastern part of the BoB. In winter, tropical cyclones tend to track towards the west and make landfall in the south-western fringe of the BoB. TCs are moving towards the west or northwestward in the monsoon season and landfall is observed in the north-western fringe of the BoB. Among the four seasons, pre- and post-monsoon season are the two-peak seasons for Bangladesh and both contribute a total of 88% landfall whereas individually the pre-monsoon season is the most concerning for Myanmar (about 66% of annual total tropical cyclones are seen to make landfall each year). The most active period (the highest percentage of landfall) for India is seen during the post-monsoon season where

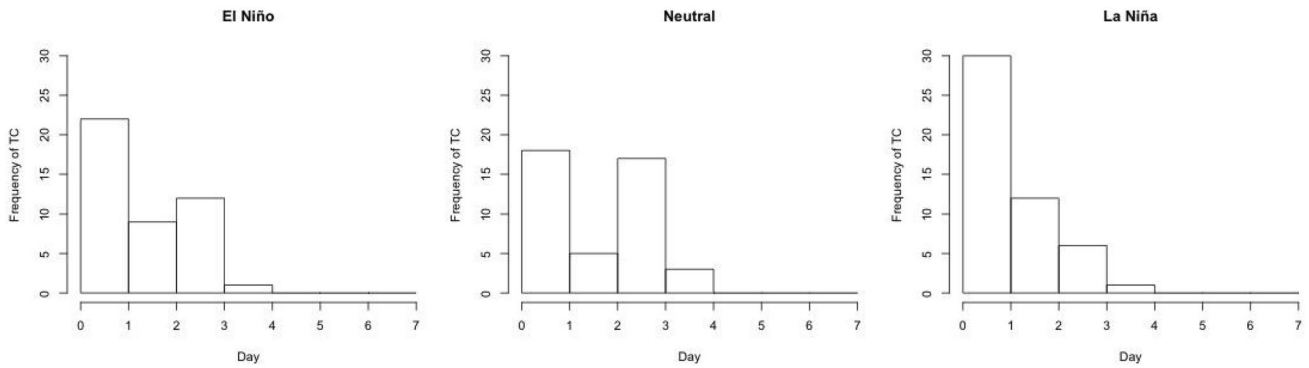


**Fig. 7** Simulated TC landfall frequency from genesis to landfall (1980–2009) for each ENSO phase binned by the time to landfall in days

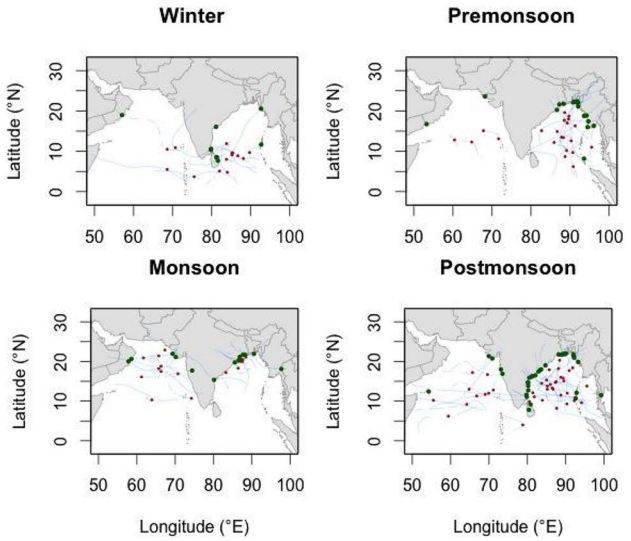


**Fig. 8** Seasonally stratified observed TC formation (red dots), trajectories (blue lines), and landfall positions (green dots) for 30-year period (1980–2009) in the NIO

71% of annual TCs landfall is observed. For Sri Lanka, the highest percentage of annual landfall occurred during winter, and whereas, for Oman, the maximum annual landfall is seen during the monsoon season.

### 3.4 Tropical cyclone activity jointly by season and ENSO phase

Modelled TCs activity by season and ENSO phase are shown in Fig. 9. In El Niño phase, TCs are moving towards a northward and northeastward direction over the BoB during winter and pre-monsoon, and landfall is seen in the eastern part of the BoB, especially Chittagong in Bangladesh and the Irrawaddy coast of Myanmar. However, cyclones move towards the north or westward during the monsoon and post-monsoon season and maximum landfalls are observed along the Tamil Nadu and Andhra Pradesh in India and a few are in the western fringe of Bangladesh. Over the BoB and the AS, during the winter, monsoon and post-monsoon seasons in the neutral phase, TCs move westward and landfalls are seen in Sri Lanka (during winter) and along the Orissa (in monsoon) and Andhra Pradesh (in post-monsoon) coast of India. However, north-eastward movement with landfall in Chittagong of Bangladesh and Myanmar is seen in the post-monsoon season. During the La Niña phase for all seasons, storms move westward and northwestward in the BoB and the Arabia Sea (AS) and make landfall along east India (Andhra Pradesh, Orissa and Tamil Nadu) and the southern fringe of Bangladesh.

The modelled distribution of genesis points for individual seasons in each ENSO phase is shown in Fig. 10. In boreal winter, for all three phases of ENSO, the highest densities are seen in 5°–10° in the both BoB and AS, while the highest genesis densities are closer to 10°–20° (10°–15°) in the BoB (AS) in the pre-monsoon season. On the other hand, the highest densities are found in 15°–20° (10°–20°) in the BoB (AS) during monsoon season, whereas the post-monsoon shows the highest densities in 10°–20° for the BoB and the AS for all three phases of ENSO.

Figure 11 shows the distribution of TC velocities for each ENSO phase. During winter in El Niño phase, a northeastward movement is seen in the NIO whereas the westward movement and later recurving towards the east movement is seen in both Neutral and La Niña phase. During pre-monsoon season, each phase shows different characteristics of movement for example the velocity field is seen towards the north in El Niño phase, eastward in Neutral phase and westward (later eastward) during La Niña phase in the BoB, whereas for the AS, the velocity field is seen towards the north-west (west) in El Niño and Neutral (La Niña) phase. During monsoon and post-monsoon, the velocity field indicates a westward movement for all three phases of ENSO except post-monsoon La Niña phase in which their movement turns west to east.

Model simulations of TC tracks (Fig. 12) as a function of both season and ENSO phase display the movement of trajectories and their point of landfall. During the winter and pre-monsoon El Niño phase, tropical cyclones tend to track towards northeastward over the BoB and the majority make landfall in the eastern part of the BoB, especially Chittagong–Cox's bazar coast in Bangladesh and the coastal zone of Myanmar. However, cyclones move towards the north during the monsoon and most of them make landfall along the coastal fringe of Bangladesh, and during the post-monsoon season cyclones move westward where they make landfall along the east coast of India. Over the AS, during the El Niño phase for all four seasons except the winter, storms move westward and make landfalls in the coastal fringe of Oman. This is generally consistent with observations. During the Neutral phase, a majority of storms move northwards over the BoB in winter, eastwards in the pre-monsoon, both eastwards and westwards in monsoon and west in the post-monsoon season. For all four seasons in La Niña phase, western movement is observed (consistent with observations) in the BoB and make landfalls along the Tamil Nadu, Andhra Pradesh in India and also the southeastern part of Bangladesh for monsoon and Myanmar for post-monsoon. Whereas over the AS, cyclone movement varies with seasons (consistent with observations).

### 3.5 TC movement mechanism

The driving force of steering flow determines the movement of TCs (Fadnavis et al. 2014). In this paper, we used

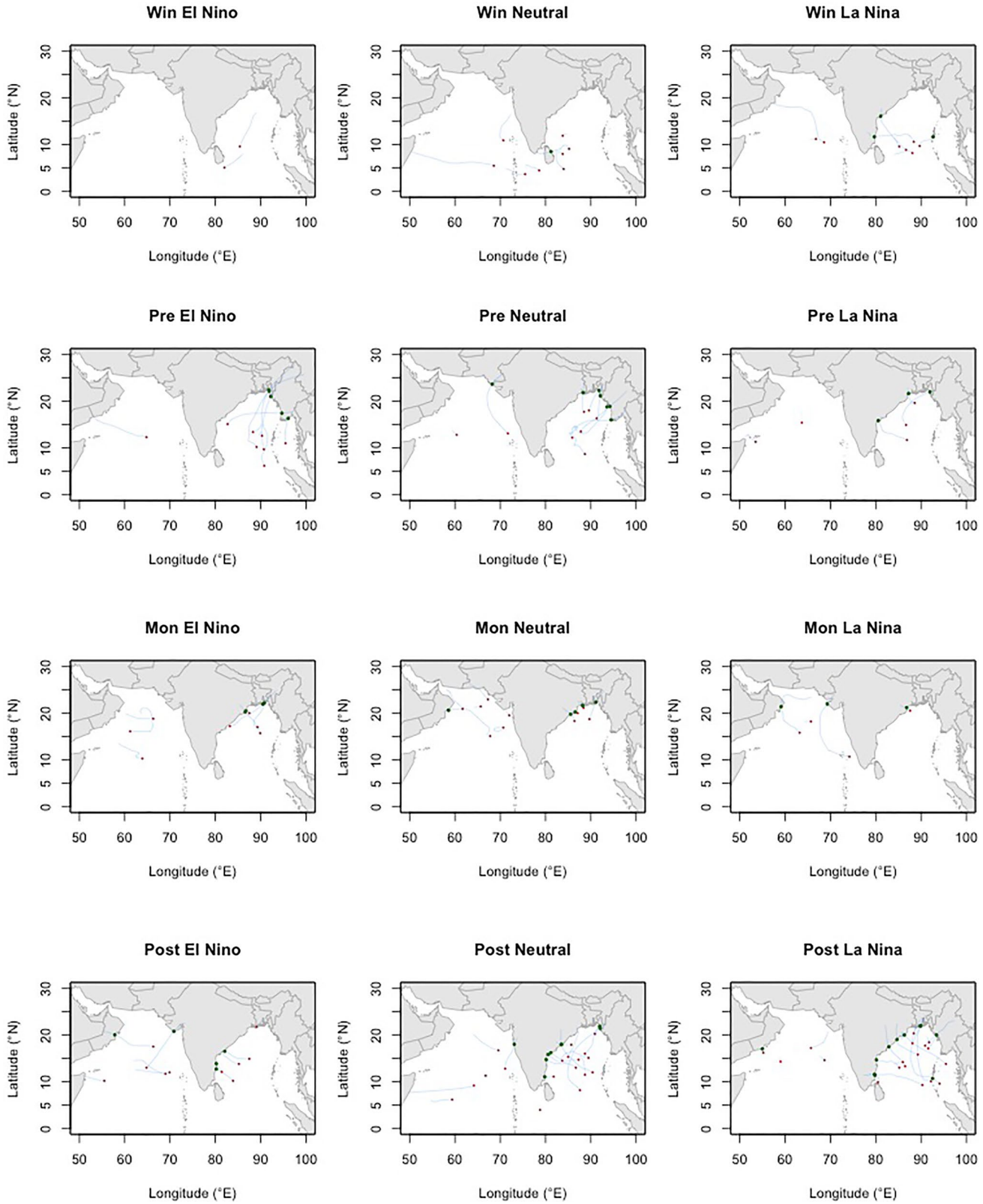


**Fig. 9** Observed TC genesis (red dots), movement (blue lines) and landfall (green dots) during different seasons in El Niño years (left), Neutral (middle) and La Niña (right)

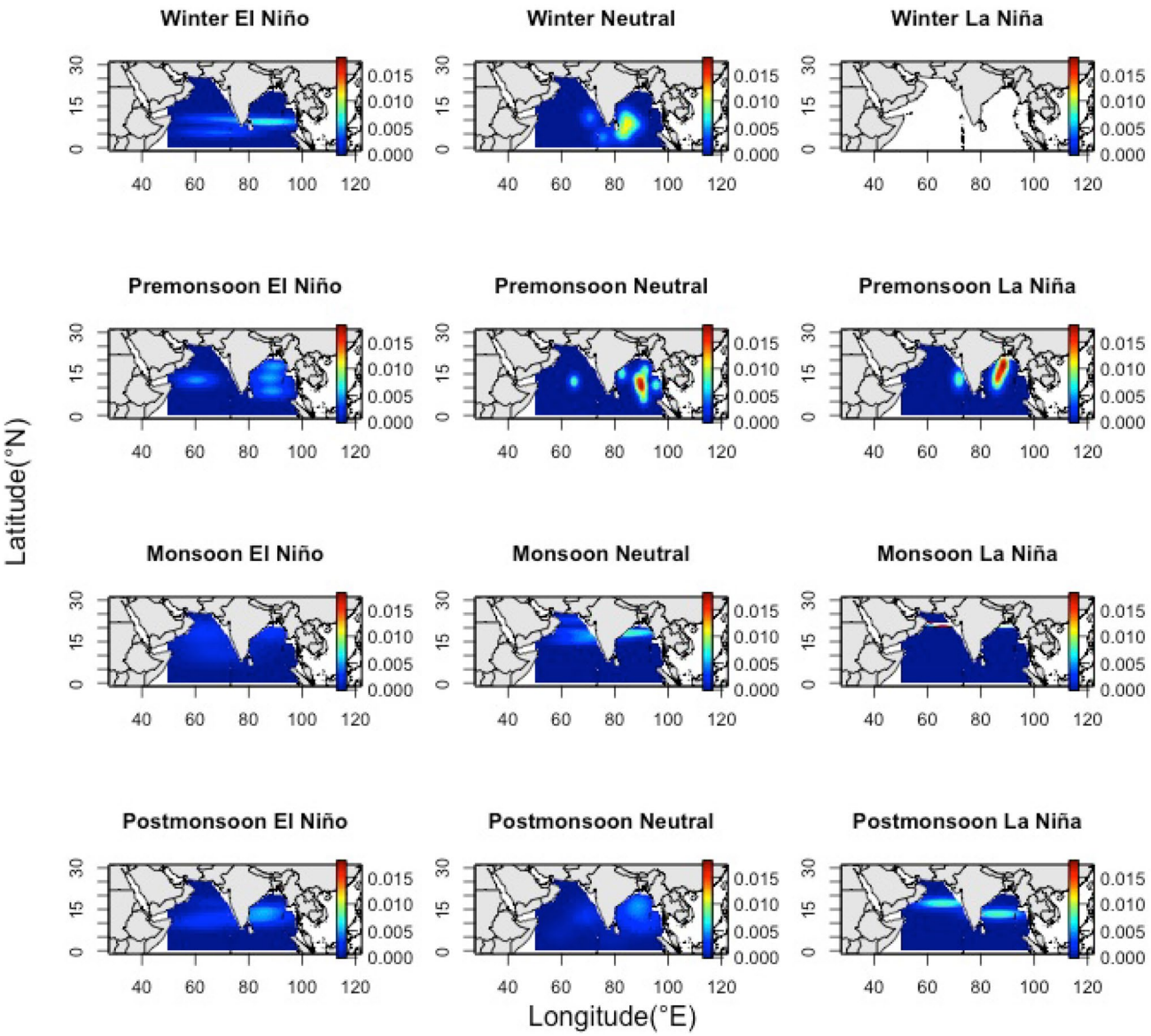


**Fig. 10** Modelled distribution of TC genesis locations in the NIO for the El Niño (left), Neutral (middle) and La Niña (right) phases of the ENSO in different seasons based on the 30-year period 1980–2009. Red color shows the highest density (concentration of TC numbers/km$^2$) area of TC formation

500 hpa wind to show TC motion during ENSO phase based on the findings of earlier studies by Girishkumar and Ravichandran (2012) and George and Gray (1976). Figure 13 shows the wind pattern of El Niño, Neutral and La Niña phase during pre and post-monsoon season across the Bay of Bengal and Arabian sea. Wind pattern indicates northeast (westward and northwestward) movement in pre (post)-monsoon season which is consistent with the TC track model's results.

### 3.6 Model validation and forecast skill

The model was validated by leave-one-out cross-validation (LOOCV) and distance calculation. Using the LOOCV with majority vote approach for a climatological model, Wahiduzzaman et al. (2017) found that the prediction of model compared well with observation. The distance validation approach (Fig. 14) shows that the maximum simulated TC landfall (68.8%) occurred within 500 km

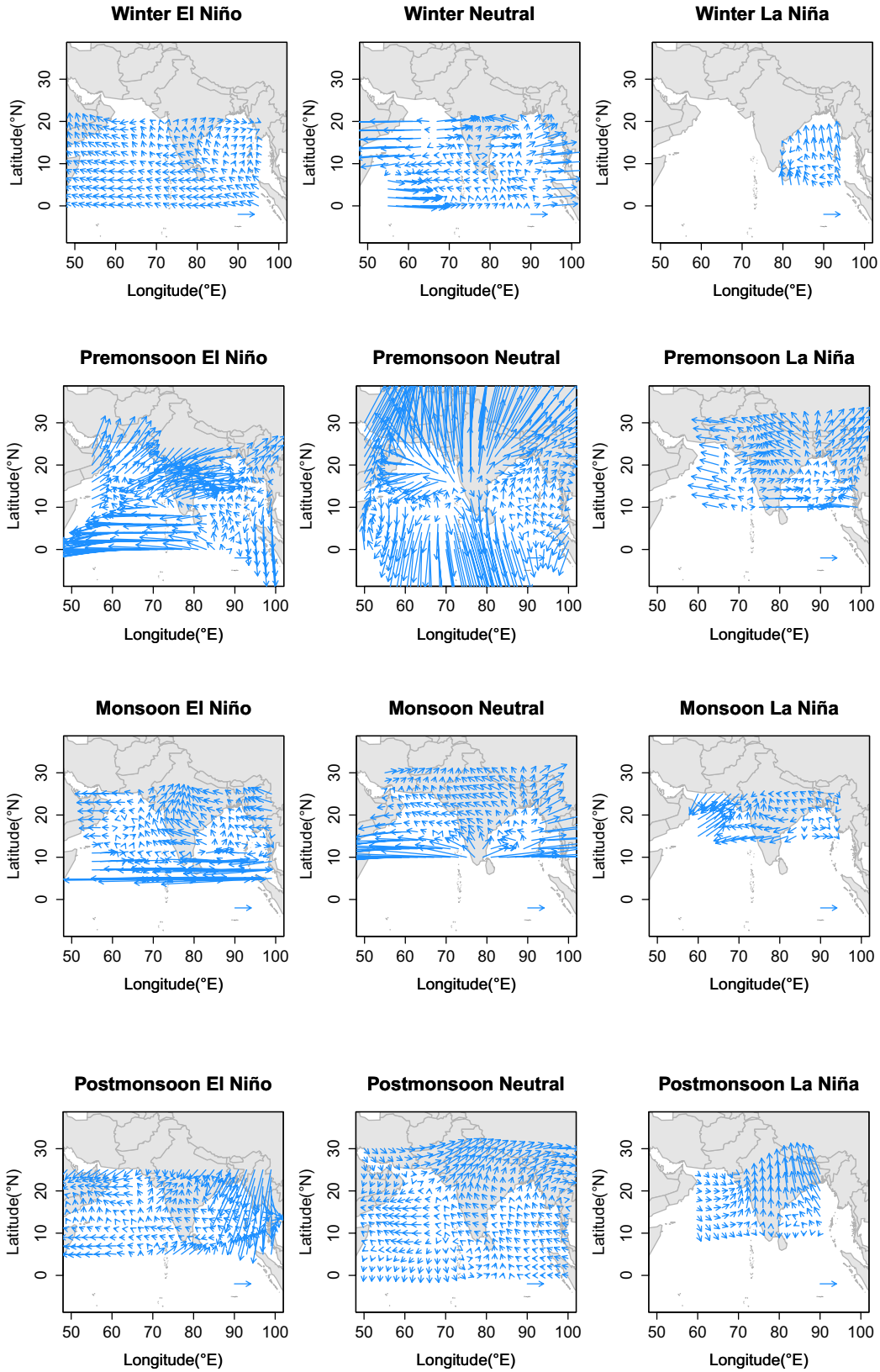


**Fig. 11** Velocities of TC track for El Niño, Neutral and La Niña phase in different seasons (winter, pre-monsoon, monsoon and post-monsoon). Reference arrow denotes 10m/s

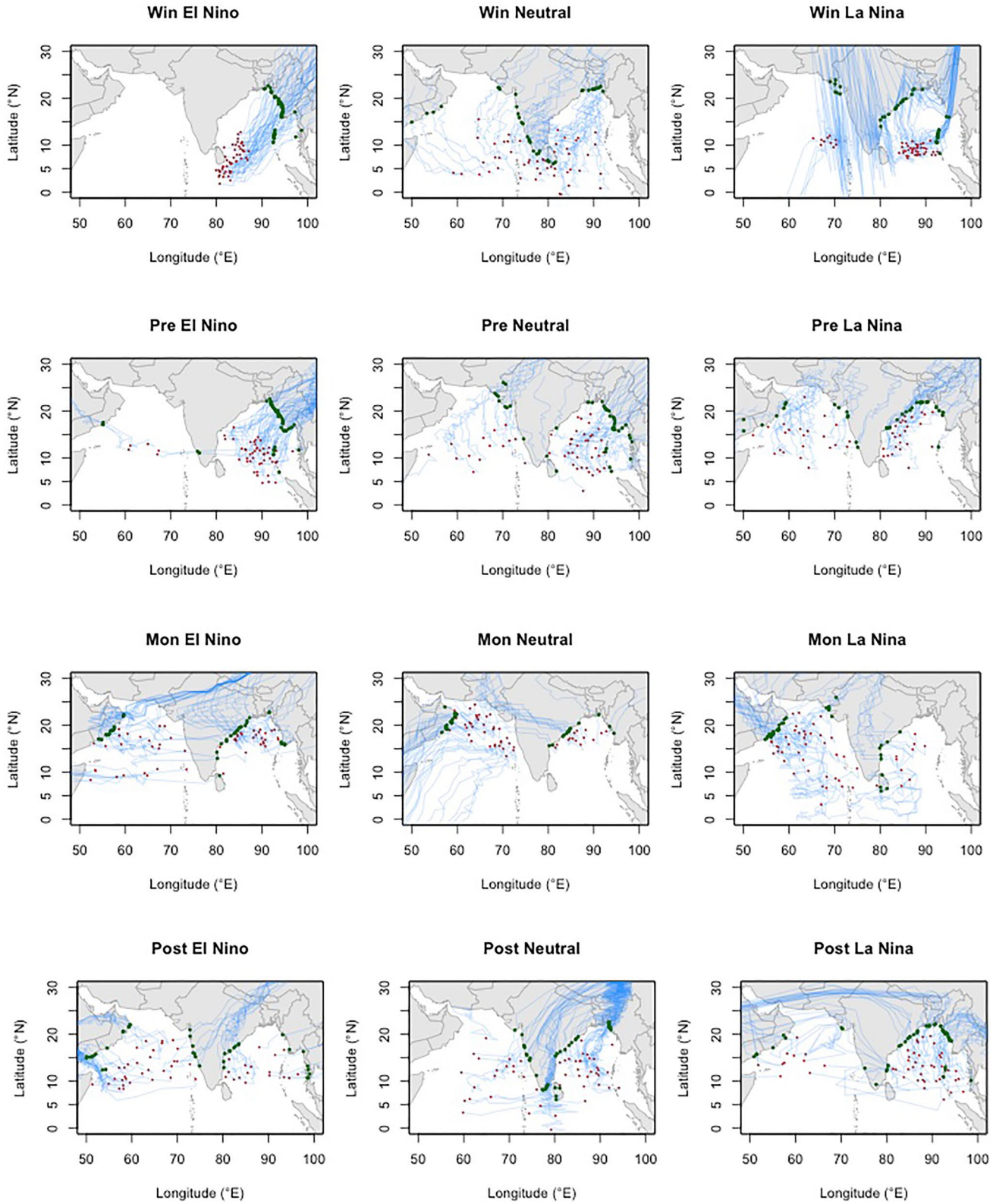


**Fig. 12** Simulated TC formation, trajectories and landfall during four seasons over the NIO for the El Niño (left), Neutral (middle) and La Niña (right) phases of the ENSO. Red (green) dots show the TC genesis (landfall) point in the NIO region (0°–30° N and 50°–100° E) for a 30-year period from 1980 to 2009. The blue lines indicate the TC trajectories

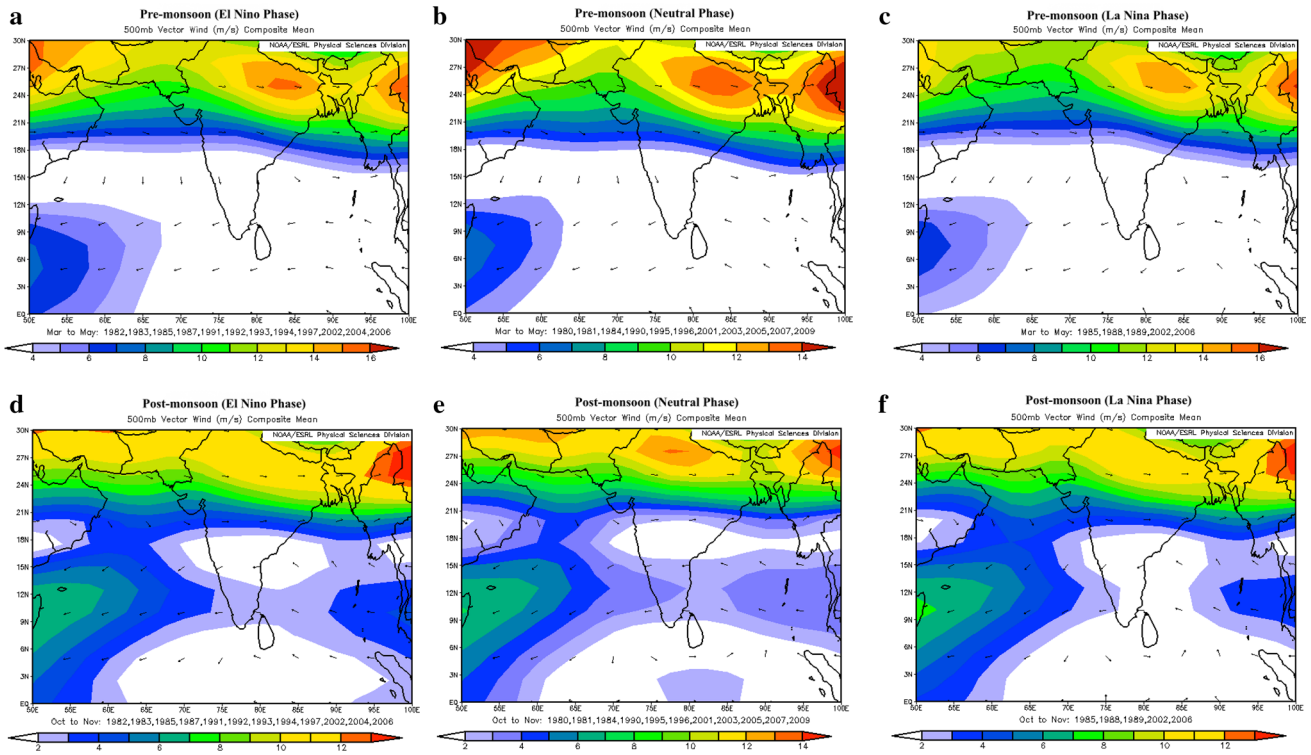


**Fig. 13** Distribution of 500 hPa winds (m/s) for ENSO phase during pre-monsoon season (**a**–**c**) and post-monsoon season (**d**–**f**) (figure reproduced from Wahiduzzaman and Yeasmin 2019b)

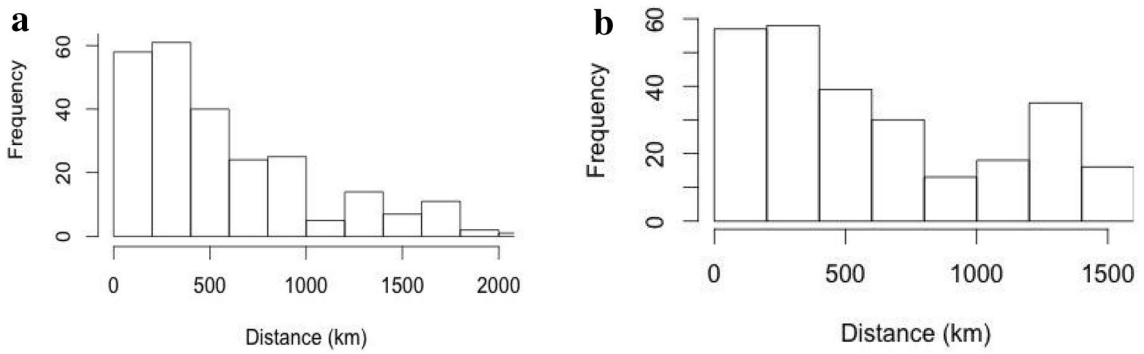


**Fig. 14** Distribution of distances **a** based on climatology prediction, **b** when ENSO is considered as a predictor

which is skillful in consideration of the median storm size (Chavas et al. 2016).

To assess the model skill, a comparison between observation and the model simulation is presented in Table 3. The model simulation considered both climatology and ENSO predictor. The seasonal forecast model is found to perform well in comparison with climatological model. The forecast model predicted very well for Myanmar (5.7%) and Sri Lanka (2.3%) (consistent with observations). The climatology is showing a very good skill for India and Oman (consistent with observation).

The distance calculation approach shows a 68.8% (63.3%) of total TC landfalls were within 500 km by forecast model (climatological model) so the forecast model claims approximately 15% improvement (Skill score = $\text{Score}_{\text{forecast}} - \text{Score}_{\text{reference}}/\text{Score}_{\text{perfect forecast}} - \text{Score}_{\text{reference}} = (68.8 - 63.3/100 - 63.3) = (5.5/36.7) = 15\%$) over climatology (Fig. 14).

The skill of model forecast has been further evaluated over the 2010–2013 period, using the 1980–2009 period for the model fit. During this period TCs occurrence has been found in winter (2011), pre-monsoon (2010 and 2013)

and post-monsoon (2010–2012). The observation, model forecast and model anomalies (forecast model–climatological model) are shown in Fig. 15. In the 2010 pre-monsoon period, observed landfall is seen in Andhra Pradesh of India, Oman (Fig. 15a) and the model forecasted the highest probability in Andhra Pradesh and Orissa in India, Rakhine in Myanmar (Fig. 15b). The forecast model minus climatology (Fig. 15c) showed a maximum increased (decreased) likelihood in Andhra Pradesh and Orissa of India (Ayeyarwady, Myanmar). For post-monsoon period, observed landfall is seen in Rakhine of Myanmar (Fig. 15d) and the model forecasted maximum probabilities along the Myanmar coast (Fig. 15e). The forecast model minus climatology showed a maximum increased likelihood along the Myanmar coast with a decreased likelihood along the eastern part of India coast (Fig. 15f).

In winter season 2011, TC made landfall in Tamil Nadu of India (Fig. 15g) and the model predicted landfall in Sri Lanka as well as Tamil Nadu of India (Fig. 15h). Probability was more in Sri Lanka and less in Tamil Nadu of India than climatological model (Fig. 15i). For post-monsoon, observed landfall is seen in Chittagong of Bangladesh as well as Dofar in Oman (Fig. 15j) and the model predicted maximum probabilities along the east coast of Bangladesh as well as Myanmar (Fig. 15k). The forecast model minus climatology showed a maximum increased likelihood along the Bangladesh (east coast)-Myanmar coast with a decreased likelihood along the eastern part of India coast as well as Dofar in Oman (Fig. 15l).

During 2012 post-monsoon period, TC made landfall in Andhra Pradesh of India (Fig. 15m) and the model forecasted highest probabilities along the Myanmar coast followed by Andhra Pradesh, India (Fig. 15n) where positive anomalies were seen in Myanmar coast and negative anomalies in east coast of India (Fig. 15o).

In 2013 pre-monsoon season, observed landfall is seen in Chittagong coast of Bangladesh (Fig. 15p) and the model predicted maximum probabilities in Chittagong of Bangladesh, Rakhine of Myanmar, Andhra Pradesh and Orissa of India (Fig. 15q) where these regions showed positive anomalies and maximum negative anomalies are found in Barisal coast of Bangladesh and Ayeyarwady of Myanmar (Fig. 15r). Overall, the model did well for the year of 2010 (pre and post monsoon), 2011 (post-monsoon), 2013 (pre-monsoon) and worse for the year of 2011 (winter season), 2012 (post-monsoon season) compared to climatological model.

**Fig. 15** TC landfall probabilities during **a–c** 2010 pre-monsoon; **d–f** ▶ 2010 post-monsoon; **g–i** 2011 winter; **j–l** 2011 post-monsoon; **m–o** 2012 a post-monsoon and **p–r** 2013 pre-monsoon. Left (middle) column shows the observation (model prediction) and the difference between forecast model and climatology is shown by right column

By averaging all the validation results we draw maps to focus the probabilities by forecast model as well as the difference with climatological model. The pre and post-monsoon (two major peak seasons) observation, model forecast and model anomalies (forecast model–climatological model) are shown in Fig. 16. In pre-monsoon El Niño phase, TC made landfall in Rakhine of Myanmar (Fig. 16a) and the model forecasted maximum landfall probabilities along the Myanmar coast (Fig. 16b) with positive anomalies in Ayeyarwady of Myanmar and negative anomalies in Rakhine of Myanmar and Andhra Pradesh and Orissa of India (Fig. 16c). During the Neutral phase, TC made landfall in Chittagong of Bangladesh, Rakhine of Myanmar (Fig. 16d) and the model forecasted well in these regions (Fig. 16e) and positive anomalies are seen in Chittagong of Bangladesh (Fig. 16f). In La Niña phase, TC landfall is seen in West Bengal of India (Fig. 16g) which is predicted well by forecast model (Fig. 16h) compared to climatology (Fig. 16i).

During post-monsoon El Niño phase, TC made landfall in Andhra Pradesh of India and Oman (Fig. 16j) and we found model predicts maximum (positive anomalies) in these regions (Fig. 16k) and negative anomalies are found in West Bengal of India (Fig. 16l). In Neutral phase, maximum landfall is seen in east coast of India (Fig. 16m) and the

**Table 3** Observed and simulated TCs number and percentages using climatology and ENSO as a predictor

| Country | Observation | | Simulation (climatology) | | Simulation (forecast model | |
|---|---|---|---|---|---|---|
| | No | % | No | % | No | % |
| India | 34 | 38.6 | 38 | 43.2 | 53 | 60.2 |
| Myanmar | 7 | 7.9 | 1 | 1.1 | 5 | 5.7 |
| Bangladesh | 14 | 15.9 | 0 | 0 | 2 | 2.3 |
| Sri Lanka | 3 | 3.4 | 16 | 18.2 | 2 | 2.3 |
| Oman | 5 | 5.7 | 3 | 3.4 | 11 | 12.5 |
| Yemen | 0 | 0 | 2 | 2.3 | 4 | 4.5 |
| Sum | 63 | 71.6 | 60 | 68.2 | 77 | 87.5 |
| NON | 25 | 28.4 | 28 | 31.8 | 11 | 12.5 |
| Total | 88 | 100 | 88 | 100 | 88 | 100 |

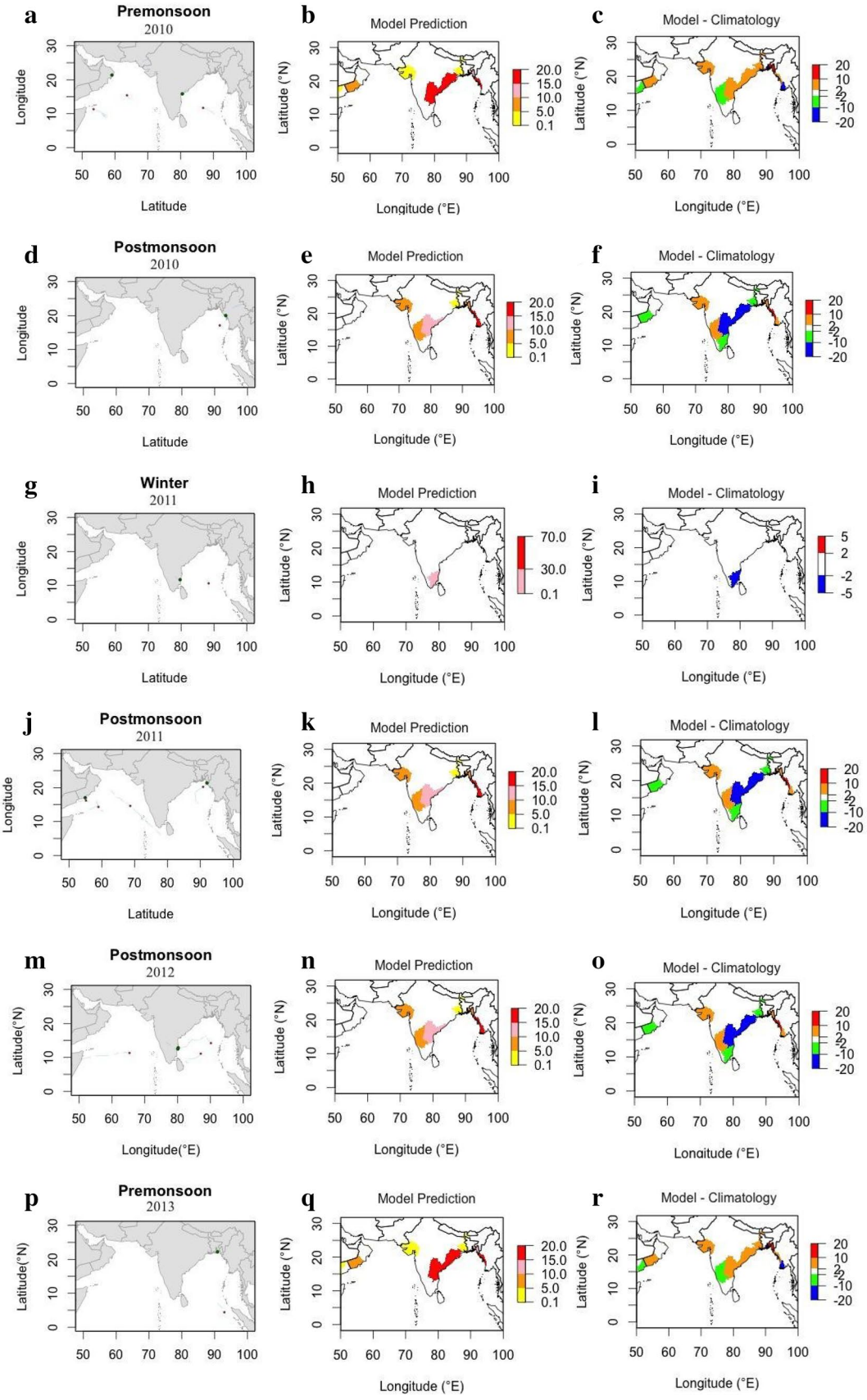
a
Premonsoon
2010
Longitude
Latitude
b
Model Prediction
Latitude (°N)
Longitude (°E)
20.0
15.0
10.0
5.0
0.1
c
Model - Climatology
20
10
2
-2
-10
-20
d
Postmonsoon
2010
e
Model Prediction
f
Model - Climatology
g
Winter
2011
70.0
30.0
0.1
h
Model Prediction
i
Model - Climatology
5
2
-2
-5
j
Postmonsoon
2011
k
Model Prediction
l
Model - Climatology
m
Postmonsoon
2012
Latitude(°N)
Longitude(°E)
n
Model Prediction
o
Model - Climatology
p
Premonsoon
2013
q
Model Prediction
r
Model - Climatology

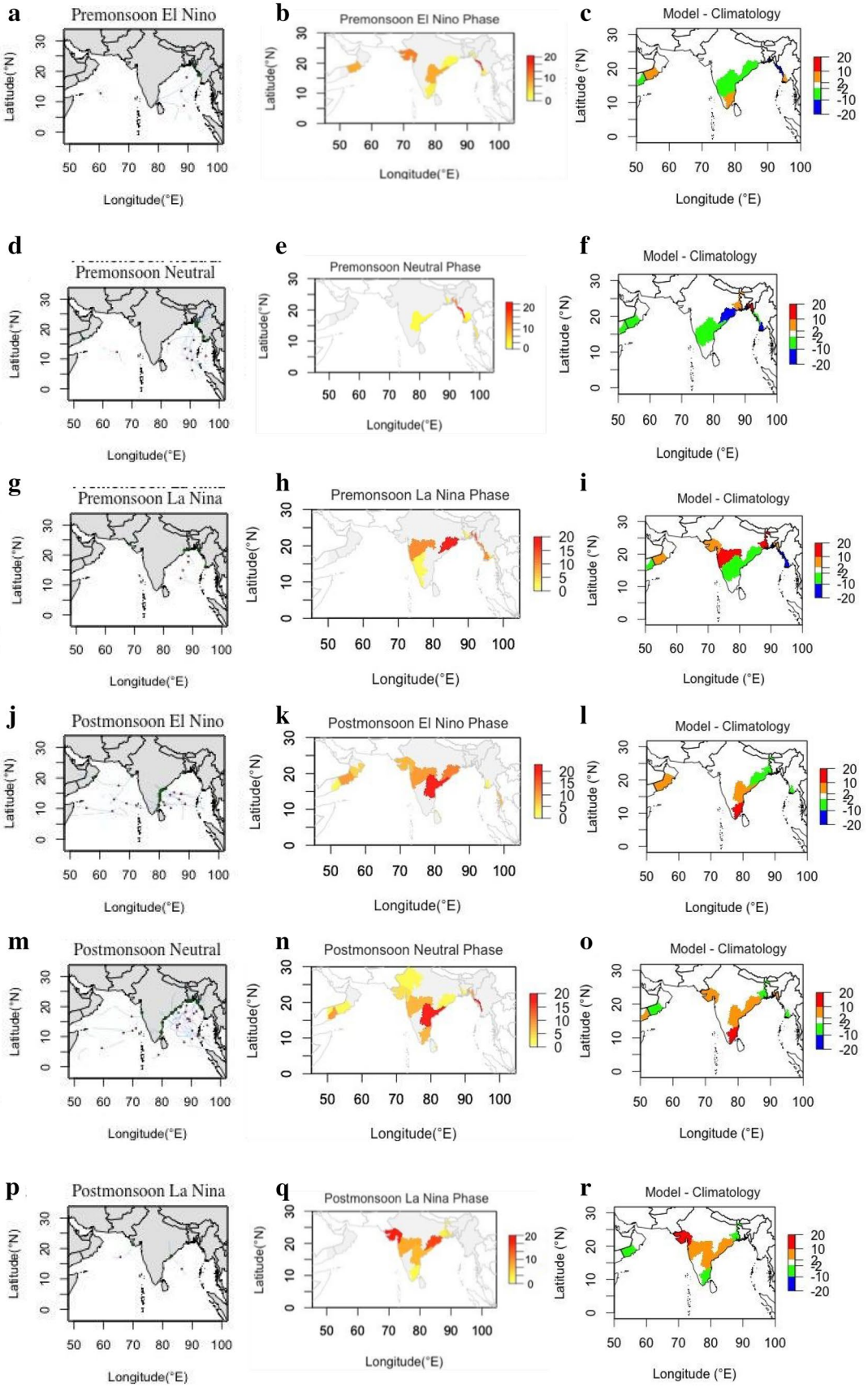
a
Premonsoon El Nino
b
Premonsoon El Nino Phase
c
Model - Climatology
d
Premonsoon Neutral
e
Premonsoon Neutral Phase
f
Model - Climatology
g
Premonsoon La Nina
h
Premonsoon La Nina Phase
i
Model - Climatology
j
Postmonsoon El Nino
k
Postmonsoon El Nino Phase
l
Model - Climatology
m
Postmonsoon Neutral
n
Postmonsoon Neutral Phase
o
Model - Climatology
p
Postmonsoon La Nina
q
Postmonsoon La Nina Phase
r
Model - Climatology
Latitude(°N)
Longitude(°E)

◂**Fig. 16** TC landfall probabilities for **a–c** pre-monsoon and El Niño phase; **d–f** pre-monsoon and neutral phase; **g–i** pre-monsoon and La Niña phase; and **j–l** post-monsoon and El Niño phase; **m–o** post-monsoon and Neutral phase; and **p–r** post-monsoon and La Niña phase. Results have been accumulated across 30-years of leave-one-out cross validation. Left (middle) column shows the observation (model prediction) (middle) and the difference between forecast model and climatology is shown in right column

model predicted maximum probabilities along the coast of Myanmar as well as south east of India (Fig. 16n). The forecast model minus climatology showed a maximum increased likelihood along the east coast of India except West Bengal (Fig. 16o). During La Niña phase, TC made landfall in Gujarat and Andhra Pradesh of India (Fig. 16p) and the model forecasted well in these regions (Fig. 16q) with positive anomalies (Fig. 16r).

## 4 Discussion and summary

The climate of the Indian Ocean region is strongly influenced by ocean variability on various spatial and temporal scales (Schott and McCreary 2001). Tropical cyclone activity over the North Indian Ocean is influenced by El Niño-Southern Oscillation (Girishkumar et al. 2015), the Quasi-Biennial Oscillation (Fadnavis et al. 2014), the Pacific Decadal Oscillation (Girishkumar et al. 2014), the Boreal Summer Intraseasonal Oscillation (Kikuchi and Wang 2010), the Indian Ocean Dipole (Saji et al. 1999), and the Madden–Julian Oscillation (Kikuchi and Wang 2010; Girishkumar et al. 2015), and so on. This paper investigates the relationship between the El Niño-Southern Oscillation and TC frequency and tracks, and discusses the development and performance of a statistical seasonal forecast model. ENSO is effectively phase-locked to the seasonal cycle (Bengtsson et al. 2007; Li et al. 2010). Typically, the developing ENSO-event during September–October–November has more influence on post-monsoon TCs. ENSO also has much less predictability, especially during March–April–May associated with the "springtime predictability barrier". One benefit of this model is the potential for forecasts months in advance.

This paper developed a statistical seasonal forecast model of TCs activities over the NIO using ENSO as a predictor. The paper addresses questions and carries out analyses using a variety of statistical methods and climate analysis tools for the seasonal forecast models. Girishkumar and Ravichandran (2012), Ng and Chan (2012), Felton et al. (2013) and Mahala et al. (2015) have shown a potential relationship between ENSO and TC over the BoB. Building on these recent research findings, we have used Kernel density estimation to model the TC genesis points, then Generalised Additive Model to model the TC tracks.

We have endeavoured to be both pragmatic and consistent with TC data reliability for the NIO region. This choice from 1979 for TCs in the model is based on both reported research (Weinkle et al. 2012; Wahiduzzaman et al. 2017, 2019) and our own analysis of historical NIO region TC observations. Unfortunately, there are many issues with the data over the NIO prior to 1979, due to lack of geostationary satellite data and limited observations, and so we considered it important not to extend our analysis prior to 1979. Instead, we addressed the issue of data paucity, and examined statistical significances of our results (Wahiduzzaman et al. 2019). Two-sample Student's $t$ test has been applied on the time series of the number of cyclones for the entire NIO and it is found that the landfall frequency is significantly different at 95% confidence level for all ENSO phase.

During a 30-year period (1980–2009), a total number of 88 TCs have been observed, and among them, 63 TCs (71.6%) made landfall across the six NIO rim countries. For the ENSO phase, the highest average frequency of genesis is seen in the La Niña years (3.67), whereas El Niño and the Neutral years correspond to the 2.9 and 2.76 respectively over the NIO. There is a significant change for the cyclonic movement during both seasons and ENSO phase and the landfall probabilities for each phase of ENSO and season varies.

During El Niño (La Niña), the GAM -fitted velocity field highlights the westward/northwestward (northeastward) direction. TC tracks, when stratified as per the phase of ENSO, show the evidence of an influence of ENSO on the movement and landfall. For example, during El Niño phase, cyclones move south of 17° N where they move north of 15° N in La Niña phase to make landfall. Overall, during El Niño (La Niña) years most of geneses have been observed in the western (eastern) Bay of Bengal and landfall in the east coast of India, particularly Tamil Nadu and Andhra Pradesh (Orissa coast of India and the southwestern fringe of Bangladesh).

Two cross validation methods have been applied in this study. Using leave-one-out cross-validation, the model shows approximately 70% skill for matching simulated landfall with observed landfall. The distance calculation approach demonstrates that the model is relatively skillful (approximately 64% skill) considering the typical spatial scale of TCs (~ 1000 km). The global median size of a cyclone is 300 km and it is 287 km in the NIO (Chavas et al. 2016). Majority of the modelled TCs landfall occurrences were within short distance (0–300 km) of the observed landfall locations which demonstrate the model is skillful. It is within the error estimate by physical scale of TCs and dynamical model's typical error scale. The developed model performed well for the NIO rim countries; for example, it shows an excellent skill for Myanmar and Sri Lanka (very close to observations). Also, the model was skillful for individual year forecast including the highest probabilities in Andhra Pradesh of India, Rakhine of Myanmar for 2010; Chittagong

of Bangladesh in 2011 and 2013 which are consistent with observations. In our knowledge, there is no statistical model that used lead–lag analysis for ENSO as a predictor for TCs in the NIO and such we developed a statistical seasonal forecast model. By performing sensitivity analysis, lead–lag confirms ENSO is a good predictor for 2-month advance to forecast. The model was skillful and performed with a 15% improvement over the climatological model.

**Acknowledgements** Tasmania Graduate Research Scholarship from the University of Tasmania, Australia and Postdoctoral Research Funding from Nanjing University of Information Science and Technology, China supported Md Wahiduzzaman. Authors are thankful to Professor Neil J Holbrook and anonymous reviewers for their helpful discussion which improved the quality of the paper.

## References

Alam MM, Hossain MA, Shafee S (2003) Frequency of Bay of Bengal cyclonic storms and depressions crossing different coastal zones. Int J Climatol 23(9):1119–1125

An S-I, Kug J-S, Timmermann A, Kang I-S, Timm O (2007) The influence of ENSO on the generation of decadal variability in the North Pacific. J Clim 20(4):667–680

Ashok K, Saji N (2007) On the impacts of ENSO and Indian Ocean dipole events on sub-regional Indian summer monsoon rainfall. Nat Hazards 42(2):273–285

Balaguru K, Taraphdar S, Leung LR, Foltz GR (2014) Increase in the intensity of postmonsoon Bay of Bengal tropical cyclones. Geophys Res Lett 41(10):3594–3601

Bengtsson L, Hodges KI, Esch M (2007) Tropical cyclones in a T159 resolution global climate model: comparison with observations and re-analyses. Tellus Ser A Dyn Meteorol Oceanogr 59A(4):396–416

Camargo SJ (2013) Global and regional aspects of tropical cyclone activity in the CMIP5 models. J Clim 26(24):9880–9902

Camargo SJ, Barnston AG (2009) Experimental dynamical seasonal forecasts of tropical cyclone activity at IRI. Weather Forecast 24(2):472–491

Camargo SJ, Barnston AG, Zebiak SE (2005) A statistical assessment of tropical cyclone activity in atmospheric general circulation models. Tellus Ser A Dyn Meteorol Oceanogr 57(4):589–604

Camargo SJ, Emanuel KA, Sobel AH (2007) Use of a genesis potential index to diagnose ENSO effects on tropical cyclone genesis. J Clim 20(19):4819–4834

Camp J, Roberts M, Maclachlan C, Wallace E, Hermanson L, Brookshaw A, Arribas A, Scaife AA (2015) Seasonal forecasting of tropical storms using the Met Office GloSea5 seasonal forecast system. Q J R Meteorol Soc 141(691):2206–2219

Chand SS, Walsh KJE (2011) Influence of ENSO on tropical cyclone intensity in the Fiji region. J Clim 24(15):4096–4108

Chavas DR, Lin N, Dong W, Lin Y (2016) Observed tropical cyclone size revisited. J Clim 29(8):2923–2939

Chu P-S (2004) ENSO and tropical cyclone activity. Hurricanes and typhoons: past, present, and potential. Columbia University Press, New York, pp 1–494

Du YG, Song JJ, Tang JP (2013) Impacts of different kinds of ENSO on landfalling tropical cyclones in China. J Trop Meteorol 19(1):39–48

Emanuel K, Ravela S, Vivant E, Risi C (2006) A statistical deterministic approach to hurricane risk assessment. Bull Am Meteorol Soc 87(3):299–314

Fadnavis S, Ernest Raj P, Buchunde P, Goswami BN (2014) In search of influence of stratospheric Quasi-Biennial Oscillation on tropical cyclones tracks over the Bay of Bengal region. Int J Climatol 34(3):567–580

Felton CS, Subrahmanyam B, Murty VSN (2013) ENSO-modulated cyclogenesis over the Bay of Bengal. J Clim 26(24):9806–9818

George JE, Gray WM (1976) Tropical cyclone motion and surrounding parameter relationships. J Appl Meteorol 15(12):1252–1264

Girishkumar MS, Ravichandran M (2012) The influences of ENSO on tropical cyclone activity in the Bay of Bengal during October–December. J Geophys Res Oceans 117:C2033

Girishkumar MS, Thanga Prakash VP, Ravichandran M (2014) Influence of Pacific Decadal Oscillation on the relationship between ENSO and tropical cyclone activity in the Bay of Bengal during October–December. Clim Dyn 44(11–12):3469–3479

Girishkumar MS, Suprit K, Vishnu S, Prakash VPT, Ravichandran M (2015) The role of ENSO and MJO on rapid intensification of tropical cyclones in the Bay of Bengal during October–December. Theor Appl Climatol 120(3–4):797–810

Hall TM, Jewson S (2007) Statistical modelling of North Atlantic tropical cyclone tracks. Tellus Ser A Dyn Meteorol Oceanogr 59A(4):486–498

Ho CH, Kim JH, Jeong JH, Kim HS, Chen D (2006) Variation of tropical cyclone activity in the South Indian Ocean: El Niño-Southern Oscillation and Madden-Julian Oscillation effects. J Geophys Res D Atmos 111:D22

Hsu PC, Ho CR, Liang SJ, Kuo NJ (2013) Impacts of two types of El Niño and la Niña events on typhoon activity. Adv Meteorol. https://doi.org/10.1155/2013/632470

James MK, Mason LB (2005) Synthetic tropical cyclone database. J Waterway Port Coast Ocean Eng 131(4):181–192

Kikuchi K, Wang B (2010) Formation of tropical cyclones in the Northern Indian ocean associated with two types of tropical intraseasonal oscillation modes. J Meteorol Soc Jpn 88(3):475–496

Klotzbach PJ (2011) El Niño-Southern Oscillation's impact on Atlantic basin hurricanes and U.S. Landfalls. J Clim 24(4):1252–1263

Knapp KR, Kruk MC, Levinson DH, Diamond HJ, Neumann CJ (2010) The international best track archive for climate stewardship (IBTrACS). Bull Am Meteorol Soc 91(3):363–376

Kuleshov Y, Qi L, Fawcett R, Jones D (2008) On tropical cyclone activity in the Southern Hemisphere: trends and the ENSO connection. Geophys Res Lett 35(14):S08

Li RCY, Zhou W (2013) Modulation of western north pacific tropical cyclone activity by the ISO. Part II: tracks and landfalls. J Clim 26(9):2919–2930

Li T, Kwon MH, Zhao M, Kug JS, Luo JJ, Yu W (2010) Global warming shifts Pacific tropical cyclone location. Geophys Res Lett 37:L21804

Mahala BK, Nayak BK, Mohanty PK (2015) Impacts of ENSO and IOD on tropical cyclone activity in the Bay of Bengal. Nat Hazards 75(2):1105–1125

Ng EKW, Chan JCL (2012) Interannual variations of tropical cyclone activity over the north Indian Ocean. Int J Climatol 32(6):819–830

Pattanaik DR, Mohapatra M (2016) Seasonal forecasting of tropical cyclogenesis over the North Indian Ocean. J Earth Syst Sci 125(2):231–250

Rigollet P, Vert R (2009) Optimal rates for plug-in estimators of density level sets. Bernoulli 15(4):1154–1178

Ropelewski CF, Jones PD (1987) An extension of the Tahiti-Darwin Southern Oscillation Index. Mon Weather Rev 115(9):2161–2165

Rumpf J, Weindl H, Höppe P, Rauch E, Schmidt V (2007) Stochastic modelling of tropical cyclone tracks. Math Methods Oper Res 66(3):475–490

Saji NH, Goswami BN, Vinayachandran PN, Yamagata T (1999) A dipole mode in the tropical Indian ocean. Nature 401(6751):360–363

Schott FA, McCreary JP Jr (2001) The monsoon circulation of the Indian Ocean. Prog Oceanogr 51(1):1–123

Sengupta D, Senan R, Goswami BN, Vialard J (2007) Intraseasonal variability of equatorial Indian Ocean zonal currents. J Clim 20(13):3036–3055

Singh OP, Ali Khan TM, Rahman MS (2000) Changes in the frequency of tropical cyclones over the North Indian Ocean. Meteorol Atmos Phys 75(1–2):11–20

Singh OP, Ali Khan TM, Rahman MS (2001) Probable reasons for enhanced cyclogenesis in the Bay of Bengal during July–August of ENSO years. Glob Planet Change 29(1–2):135–147

Srikanth L, Ramalingam M, George MS, Bertino L, Samuelsen A (2012) A study on the influence of oceanic and atmospheric parameters on tropical cyclones in the Bay of Bengal. Eur J Sci Res 76(1):63–73

Troup AJ (1965) The southern oscillation. Q J R Meteorol Soc 91(390):490–506

Vissa NK, Satyanarayana ANV, Prasad Kumar B (2013) Intensity of tropical cyclones during pre- and post-monsoon seasons in relation to accumulated tropical cyclone heat potential over Bay of Bengal. Nat Hazards 68(2):351–371

Wahiduzzaman M, Yeasmin A (2019a) A kernel density estimation approach of North Indian Ocean tropical cyclone formation and the association with convective available potential energy and equivalent potential temperature. Meteorol Atmos Phys. https://doi.org/10.1007/s00703-019-00711-7

Wahiduzzaman M, Yeasmin A (2019b) Statistical forecasting of tropical cyclone landfall activities over the North Indian Ocean rim. Atmos Res 227:89–100

Wahiduzzaman M, Oliver ECJ, Wotherspoon SJ, Holbrook NJ (2017) A climatological model of North Indian Ocean tropical cyclone genesis, tracks and landfall. Clim Dyn 49:2585–2603

Wahiduzzaman M, Oliver ECJ, Klotzbach PJ, Wotherspoon SJ, Holbrook NJ (2019) A statistical seasonal forecast model of North Idian Ocean tropical cyclones using the Quasi-biennial Oscillation. Int J Climatol 39(2):934–952

Wang C, Wu L, Zhao H, Cao J, Tian W (2018) Is there a quiescent typhoon season over the western North Pacific following a strong El Niño event? Int J Climatol. https://doi.org/10.1002/joc.5782

Webster PJ (2008) Myanmar's deadly daffodil. Nat Geosci 1(8):488–490

Werner A, Maharaj AM, Holbrook NJ (2012) A new method for extracting the ENSO-independent Indian Ocean Dipole: application to Australian region tropical cyclone counts. Clim Dyn 38(11–12):2503–2511

Yonekura E, Hall TM (2011) A Statistical model of tropical cyclone tracks in the western North Pacific with ENSO-dependent cyclogenesis. J Appl Meteorol Climatol 50(8):1725–1739

Zhang W, Graf HF, Leung Y, Herzog M (2012) Different El Niño types and tropical cyclone landfall in East Asia. J Clim 25(19):6510–6523

Zhao H, Wu L, Wang C, Klotzbach PJ (2019) Consistent late onset of the western North Pacific tropical cyclone season following major El Niño events. J Meteorol Soc Jpn 97(3):1–17